

CATformer: Contrastive Adversarial Transformer for Image Super-Resolution

Qinyi Tian¹, Spence Cox², Laura E. Dalton^{1,*}

¹Department of Civil & Environmental Engineering, Duke University, Durham, NC, USA

²Mechanical Engineering & Materials Science, Duke University, Durham, NC, USA
{qinyi.tian@, spence.cox@, laura.dalton@}duke.edu

Abstract

Super-resolution remains a promising technique to enhance the quality of low-resolution images. This study introduces CATformer (Contrastive Adversarial Transformer), a novel neural network integrating diffusion-inspired feature refinement with adversarial and contrastive learning. CATformer employs a dual-branch architecture combining a primary diffusion-inspired transformer, which progressively refines latent representations, with an auxiliary transformer branch designed to enhance robustness to noise through learned latent contrasts. These complementary representations are fused and decoded using deep Residual-in-Residual Dense Blocks for enhanced reconstruction quality. Extensive experiments on benchmark datasets demonstrate that CATformer outperforms recent transformer-based and diffusion-inspired methods both in efficiency and visual image quality. This work bridges the performance gap among transformer-, diffusion-, and GAN-based methods, laying a foundation for practical applications of diffusion-inspired transformers in super-resolution.

Introduction

Limitations in camera hardware, cost, and physical environments often prevent the direct capture of sharp, high-resolution (HR) imagery for many scientific and industrial applications (Wang, Chen, and Hoi 2021; Yue et al. 2016). As an alternative, researchers have focused on the development of computational techniques to reconstruct high-fidelity images from low-resolution (LR) or degraded inputs as a solution to restore lost detail and expand the usefulness of visual data (Li et al. 2025; Lim et al. 2017). Over the last decade, the pursuit to improve image quality has driven profound improvements in model design and learning paradigms related to the broader context of super-resolution (SR).

Early approaches to single-image SR primarily relied on minimizing pixel-wise losses such as mean squared error (MSE), a straightforward metric for measuring pixel fidelity between the generated images and ground truth images (Ledig et al. 2017; Blau and Michaeli 2018). While effective at achieving high peak signal-to-noise ratio (PSNR) scores, these methods often produce visually unsatisfying

results where images appear to be overly smooth and/or lack the intricate high-frequency details that make real HR photographs visually appealing (Blau and Michaeli 2018). To address these shortcomings, Generative Adversarial Networks (GANs) were introduced into the SR field, marking a pivotal shift toward perceived image quality. The seminal work Super-Resolution Generative Adversarial Network (SRGAN) (Ledig et al. 2017) incorporated an adversarial loss alongside the traditional pixel-wise loss, allowing the generator to synthesize images that a discriminator would find difficult to distinguish from authentic HR images. This adversarial framework encouraged the model to reconstruct textures and details that were absent in purely MSE-optimized models. Building on this, Enhanced Super-Resolution Generative Adversarial Networks (ESRGAN) introduced significant architectural enhancements, such as the residual-in-residual dense block (RRDB) and the removal of batch normalization layers, which improved both visual sharpness and training stability (Wang et al. 2018). Real-ESRGAN (Wang et al. 2021b) further improved on these ideas by simulating more realistic and complex degradations in the training data and by leveraging U-Net-based discriminators (Ronneberger, Fischer, and Brox 2015) which enabled the model to perform robustly on challenging real-world images where degradations are unknown or mixed.

In parallel, the transformer architecture, originally designed for sequence modeling in natural language processing (Dosovitskiy et al. 2021; Vaswani et al. 2017), began to influence image restoration and SR. Transformers are distinguished by their use of self-attention, which enables them to model long-range dependencies and contextual relationships across an image. For example, the transformer-based topography neural network (TTSR) (Yang et al. 2020; Wang et al. 2024) introduced cross-scale attention mechanisms to transfer fine texture details from high-quality reference images, thereby enriching the super-resolved output. Image restoration using Swin Transformer (SwinIR) (Liang et al. 2021) adapted the Swin Transformer with shifted windowed self-attention, achieving state-of-the-art SR performance with manageable computational costs. Other models such as Efficient Super-Resolution Transformer (ESRT) (Lu et al. 2022) and Restoration Transformer (Restormer) (Zamir et al. 2022) further demonstrated the flexibility and effectiveness of transformers, introducing lighter and scalable

designs that generalized well to both SR and general image restoration tasks.

Recently, diffusion models have gained traction in SR applications by modeling the generation process as gradual denoising from random noise to a clean image. Image Super-Resolution via Iterative Refinement (SR3) (Saharia et al. 2023) was a recent breakthrough which used iterative denoising conditioned on LR inputs to reconstruct detailed HR images. This approach set a new standard for image fidelity, especially for large scaling factors. Subsequent research, include Latent Diffusion Models (LDM) (Rom-bach et al. 2022), which demonstrated the ability of diffusion models to handle high upscaling ratios (such as 16 \times and 64 \times) and to synthesize high-frequency details using specialized conditioning and network structures. Bayesian Uncertainty Guided Diffusion Probabilistic Model (BUFF) (He et al. 2025) further extended these ideas by introducing probabilistic modeling through uncertainty masks that guide noise addition spatially allowing generation of diverse HR outputs and better modeling of uncertainty in the SR process.

Recognizing the strengths of both GANs and diffusion models, hybrid frameworks have emerged to combine the advantages of both model frameworks. SupResDiffGAN (Kopeć et al. 2025) is one example, which merged diffusion-based refinement in the latent space with the fast inference and perceptual sharpness provided by GAN discriminators. This hybrid approach achieved visually impressive results with efficiency that rivaled, and even exceeded, traditional diffusion models. Beyond these main model families, contrastive learning has recently been explored as a way to enhance feature representations for SR. By learning to distinguish between positive and negative feature pairs, contrastive learning helps the model capture more discriminative and robust texture information. For instance, Wu et al. (Wu, Jiang, and Liu 2024) proposed a contrastive learning strategy to guide the generator in distinguishing subtle differences between high- and low-quality textures, resulting in improved perceptual fidelity. Similarly, Wang et al. (Wang et al. 2021a) proposed Unsupervised Degradation Representation Learning (DASR), a contrastive learning approach that learns resolution-invariant features by contrasting multiple degraded versions of an input, enabling SR networks to better generalize to unseen degradations while preserving fine details.

Informed by and building on these recent advancements in SR, this study proposes a novel, dual-branch neural architecture which unites transformer modules inspired by diffusion processes, adversarial (GAN) supervision, and contrastive learning in the latent feature space. This model, Contrastive Adversarial Transformer (CATformer), is designed to simultaneously extract multi-scale features and reconstruct high-quality outputs by integrating the iterative denoising of diffusion, the discriminative feedback of GANs, and the robust representation learning of contrastive objectives. The primary aim of this model development is to offer an effective solution which can adapt to a variety of degradations present in real-world imagery and deliver consistently sharp and perceptually convincing results.

Related Works

SR has been extensively studied through a range of generative approaches, including convolutional neural networks (CNN), GANs, and more recently, diffusion-based models. GAN-based methods such as SRGAN (Ledig et al. 2017) and ESRGAN (Wang et al. 2018) were the first examples of adversarial learning to improve perceptual quality in super-resolved images. While useful, some challenges, such as mode collapse and artifact generation, have been noted. Diffusion models, initially developed for unconditional generation, have been adapted for SR tasks to improve stability and sample diversity. SR3 (Saharia et al. 2023) demonstrated strong performance on face and general image SR by progressively refining a low-resolution image through a diffusion process. Cascaded Diffusion Models (Ho et al. 2022) extended this idea to multi-stage HR synthesis, including SR components. These methods typically use convolutional U-Net backbones during the denoising process. Transformer-based architectures have also been applied to SR to test the ability of these architectures to capture long-range dependencies. Vision Transformer (ViT) (Dosovitskiy et al. 2021) and Transformer U-Net designs (Peebles and Xie 2023) have shown promise in modeling both global structures and local details in LR vision tasks. SupResDiffGAN (Kopeć et al. 2025) introduced a hybrid framework that integrates adversarial supervision into a diffusion-based SR pipeline, improving visual fidelity through the use of a GAN discriminator. Building on these directions, the model described in this work incorporates a Transformer-based U-Net within a diffusion-inspired framework guided by adversarial feedback, with the goal to enhance both perceptual quality and global context understanding in SR.

Methodology

This work introduces CATformer, a dual-branch generative adversarial network for image SR. CATformer introduces a latent-space encoder-decoder architecture integrating transformer modules conditioned by temporal embeddings. The primary branch introduces deeper transformer-based U-Net blocks paired with extensive RRDB for detailed reconstruction, while a secondary branch introduces shallower transformer blocks with explicit noise augmentation for robustness. The method also introduces explicit fusion of latent features from both branches via channel-wise concatenation and convolution before decoding. Additionally, CATformer introduces projection heads for contrastive latent learning and a convolutional discriminator with spectral normalization to enhance perceptual realism through adversarial training.

Hierarchical Latent Encoder with Residual Refinement

The latent encoder module transforms input RGB images into compact latent feature maps through a hierarchical convolutional approach complemented by residual feature refinement. Given an input tensor $\mathbf{X} \in \mathbb{R}^{B \times 3 \times H \times W}$, the encoder produces a latent representation $\mathbf{Z} \in \mathbb{R}^{B \times 256 \times \frac{H}{8} \times \frac{W}{8}}$.

defined by:

$$\mathbf{Z} = \mathcal{E}(\mathbf{X}) = \text{RB}_3(f_3(\text{RB}_2(f_2(\text{RB}_1(f_1(\mathbf{X})))))),$$

where each convolutional stage, f_i , consists of a convolutional layer with kernel size 4×4 , stride 2, padding 1, followed by a ReLU activation function. The channel dimensions progressively increase across stages: $3 \rightarrow 64 \rightarrow 128 \rightarrow 256$.

Critically, each convolutional stage is followed by a residual block, RB_i , structured as two convolutional layers (3×3 , stride 1, padding 1) with an intermediate ReLU activation and a scaled residual connection defined as:

$$\text{RB}_i(x) = x + 0.2 \cdot \text{Conv}(\text{ReLU}(\text{Conv}(x))).$$

This residual design choice enhances gradient propagation, feature reuse, and training stability, significantly improving the capacity of the model to represent detailed structural and textural features. The underlying reason for these improvements is that the residual connections reduce the likelihood of vanishing gradients, facilitating deeper network training and more efficient optimization. Conversely, the encoder deliberately excludes normalization layers and attention mechanisms to simplify computation and reduce memory consumption, a design decision that favors computational efficiency but could introduce a scale-specific inductive bias. Such biases may limit adaptability when generalized to highly diverse visual domains or complex semantic contexts. These limitations are outside the scope of the current work and will be investigated as part of future work. Nevertheless, empirical validation demonstrates robust performance, especially when the encoder is paired with the downstream transformer-based modules that further refine global context and temporal dependencies.

Dual-Branch Architecture (After Encoder)

Following latent encoding, the representation $z \in \mathbb{R}^{B \times C_z \times H \times W}$ is processed concurrently through two complementary branches, designed to leverage deterministic refinement and robustness to noise (illustrated in Figure 1):

Branch 1: Diffusion-Inspired Transformer U-Net Latent features z are first conditioned using a temporal embedding $e_t \in \mathbb{R}^{B \times C_z}$:

$$z_{\text{diff}} = z + e_t^{\text{reshape}}.$$

These features are processed through convolutional embedding layers and reshaped into spatial tokens, allowing global context modeling through Transformer blocks:

$$\begin{aligned} z_{\text{tokens}} &= \text{reshape}(z_{\text{diff}}) \\ m &= \text{TransformerEncoder}(z_{\text{tokens}}). \end{aligned}$$

After attention-based feature extraction, tokens are reshaped back and further refined through convolutional decoding layers:

$$z_{\text{denoised}} = \text{ConvDecoder}(\text{reshape}(m), z_{\text{diff}})$$

Branch 2: Auxiliary Noise-Robust Transformer Branch

The second branch explicitly injects Gaussian noise parameterized by a noise level, σ , promoting robustness to latent perturbations:

$$z_{\text{noisy}} = z + \epsilon, \quad \epsilon \sim \mathcal{N}(0, \sigma^2).$$

These noisy latent features are processed via a shallower Transformer U-Net architecture designed to extract robust representations from noisy inputs:

$$z_{\text{noise}} = \text{NoiseTransformerUNet}(z_{\text{noisy}}, e_t^{\text{reshape}}).$$

Fusion Operation Outputs from both branches are explicitly fused through channel-wise concatenation followed by a learnable 1×1 convolution, integrating deterministic and noise-robust representations into a unified latent map:

$$z_{\text{fused}} = \text{Conv}_{1 \times 1}(\text{concat}(z_{\text{denoised}}, z_{\text{noise}})).$$

Unified Decoding and Reconstruction The fused latent representation is decoded via a deep RRDB decoder (8 RRDB blocks per stage) to generate the final super-resolved image used for evaluation and inference:

$$sr_{\text{final}} = \tanh(D_{\theta}(z_{\text{fused}})).$$

Additionally, the noise branch latent features z_{noise} are decoded via a shallower RRDB decoder (4 RRDB blocks per stage) strictly as an auxiliary output, providing regularization during training:

$$sr_{\text{aux}} = \tanh(G_{\theta}(z_{\text{noise}})) \quad (\text{regularization only}).$$

Contrastive Projection Heads Each branch employs dedicated projection heads generating compact latent vectors useful for auxiliary contrastive learning tasks:

$$v_{\text{denoised}} = P_{\text{main}}(z_{\text{denoised}}), \quad v_{\text{noise}} = P_{\text{noise}}(z_{\text{noise}}).$$

Final Outputs The complete model produces multiple complementary representations specifically supporting diverse training objectives:

$$(sr_{\text{final}}, sr_{\text{aux}}, v_{\text{denoised}}, v_{\text{noise}}, z_{\text{denoised}}, z_{\text{noise}}).$$

Discriminator A convolutional discriminator network employing spectral normalization is employed during adversarial training to further stabilize learning and enhance the perceptual realism of generated images:

$$D(x) \in \mathbb{R}^{B \times 1 \times h' \times w'}.$$

Adversarial Training and Loss Formulation

Following the dual-branch architecture, the training framework integrates adversarial learning to enhance perceptual realism. The discriminator D concurrently learns to distinguish real from generated images.

Adversarial Loss Encourages the generation of outputs indistinguishable from real images:

$$\mathcal{L}_{\text{adv}} = \text{BCEWithLogits}(D(sr_{\text{final}}), 1).$$

Pixel Reconstruction Loss Ensures fidelity at pixel level, with stronger emphasis on the main branch output:

$$\mathcal{L}_{\text{pixel}} = \|sr_{\text{final}} - z_{\text{HR}}\|_1 + \lambda_{\text{aux}} \|sr_{\text{aux}} - z_{\text{HR}}\|_1.$$

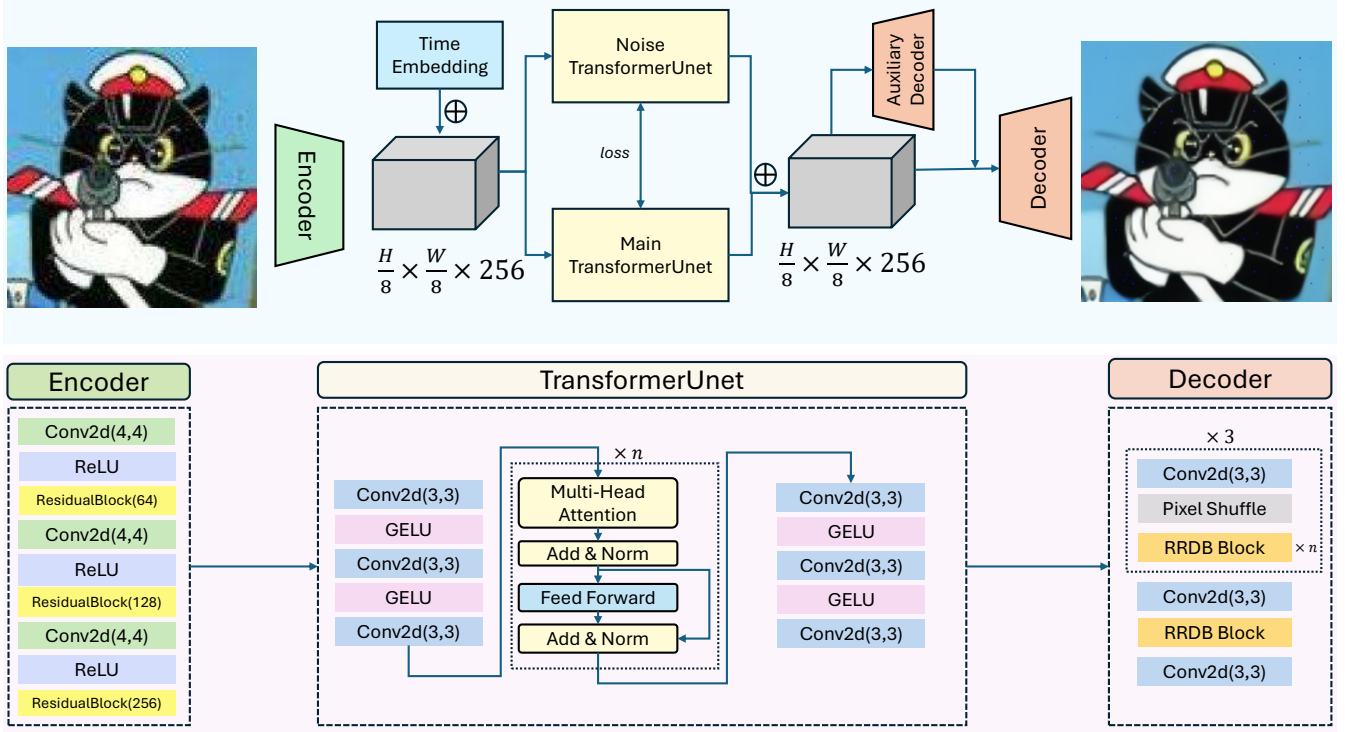


Figure 1: CATformer Architecture

LR Consistency Loss Enforces consistency with the original low-resolution inputs:

$$\mathcal{L}_{\text{LR-consist}} = \|\text{Interp}(sr_{\text{final}}) - z_{\text{LR}}\|_1.$$

Contrastive Latent Projection Loss Promotes discriminative and robust latent representations:

$$\mathcal{L}_{\text{contrastive}} = 1 - \frac{v_{\text{denoised}} \cdot v_{\text{HR}}}{\|v_{\text{denoised}}\| \|v_{\text{HR}}\|}.$$

Perceptual Loss Enforces perceptual quality using LPIPS and VGG feature similarity:

$$\mathcal{L}_{\text{perceptual}} = \text{LPIPS}(sr_{\text{final}}, z_{\text{HR}}) + \lambda_{\text{VGG}} \|\text{VGG}(sr_{\text{final}}) - \text{VGG}(z_{\text{HR}})\|_1.$$

Edge-Preserving Loss Preserves image sharpness and structural details:

$$\mathcal{L}_{\text{edge}} = \|\nabla sr_{\text{final}} - \nabla z_{\text{HR}}\|_1.$$

Branch Consistency Losses Maintains coherence between both branches:

$$\mathcal{L}_{\text{latent-consist}} = \|v_{\text{denoised}} - v_{\text{noise}}\|_2^2 + \|z_{\text{denoised}} - z_{\text{noise}}\|_2^2,$$

$$\mathcal{L}_{\text{branch-consist}} = \|sr_{\text{final}} - sr_{\text{aux}}\|_2^2.$$

Unified Generator Objective These individual terms form a comprehensive generator loss function:

$$\begin{aligned} \mathcal{L}_G = & \lambda_{\text{adv}} \mathcal{L}_{\text{adv}} + \lambda_{\text{pixel}} \mathcal{L}_{\text{pixel}} + \lambda_{\text{LR}} \mathcal{L}_{\text{LR-consist}} \\ & + \lambda_{\text{contrastive}} \mathcal{L}_{\text{contrastive}} + \lambda_{\text{perceptual}} \mathcal{L}_{\text{perceptual}} \\ & + \lambda_{\text{edge}} \mathcal{L}_{\text{edge}} + \lambda_{\text{latent}} \mathcal{L}_{\text{latent-consist}} \\ & + \lambda_{\text{branch}} \mathcal{L}_{\text{branch-consist}}. \end{aligned}$$

Discriminator Objective Binary cross-entropy loss is employed for discriminator training:

$$\begin{aligned} \mathcal{L}_D = & \frac{1}{2} [\text{BCEWithLogits}(D(z_{\text{HR}}), 1) \\ & + \text{BCEWithLogits}(D(sr_{\text{final}}), 0)]. \end{aligned}$$

Joint optimization effectively guides the model towards generating perceptually realistic, structurally coherent, and semantically consistent super-resolved images.

Experiments

This section provides a comprehensive evaluation of the proposed CATformer. Comparative experiments are conducted with recent state-of-the-art models, employing several challenging benchmarks to assess both the quantitative and qualitative performance of all competing approaches. Detailed descriptions of datasets, baseline methods, experimental settings, and evaluation metrics are provided to ensure full transparency and to facilitate reproducibility.

Datasets

The CelebA-HQ dataset (Liu et al. 2015) is used as the benchmark for super-resolution evaluation, providing high-quality celebrity face images commonly adopted in generative modeling research. High-resolution (HR) and corresponding low-resolution (LR) image sets are prepared, with LR images obtained by downsampling and renaming HR images to ensure precise one-to-one correspondence. During

dataset construction, directories are scanned and valid HR-LR image pairs are identified by matching filenames (excluding any suffix such as "x4" in the LR set) and verifying image file integrity. Each image is loaded, converted to RGB, and resized uniformly to 128×128 pixels. Both HR and LR images are normalized to the $[-1, 1]$ range using a mean and standard deviation of 0.5 per channel. Any image pairs that fail to load or are found to be corrupted are excluded automatically, ensuring a consistent and high-quality dataset. For training, image pairs are batched and shuffled using a PyTorch DataLoader, resulting in a robust pipeline for both quantitative evaluation and qualitative analysis of super-resolution performance.

Experimental Setup

All models are trained and evaluated using the PyTorch framework (Paszke et al. 2019). The generator follows the described architectural specifications, with the adversarial discriminator matched in complexity to provide a balanced learning signal. For training, Adam (Kingma and Ba 2015) is used as the optimizer with a fixed learning rate of 1×10^{-4} and a batch size of 8. Model training and inference are performed on NVIDIA A5000 GPUs with mixed-precision (Mickevicus et al. 2018) enabled to accelerate computation and reduce memory usage. Model checkpoints are selected based on the best performance on a held-out validation set, using the PSNR, Structural Similarity Index (SSIM) (Wang et al. 2004), and Learned Perceptual Image Patch Similarity (LPIPS) (Zhang et al. 2018) metrics for quantitative evaluation. All models, including the proposed method and baselines, are trained with identical preprocessing, normalization, and data augmentation pipelines. For baseline comparisons, SwinIR, RealESRGAN, ESRGAN, DiffBIR, and Hybrid Attention Transformer (HAT) (Chen et al. 2023) are included, each implemented following the official repositories and recommended training procedures as described by their respective authors. Pretrained weights are used where available to reflect optimal published performance. During evaluation, all results are reported on the CelebA-HQ test split using standardized code and metrics, ensuring fair and reproducible comparison across all methods.

Evaluation Metrics

Performance assessment relies on a suite of established quantitative metrics that reflect both pixel-level fidelity and perceptual similarity.

Pixel-wise accuracy is evaluated using Peak Signal-to-Noise Ratio (PSNR) and Mean Squared Error (MSE). The MSE between a reference image I and a reconstructed image \hat{I} of size $N \times M$ is defined as:

$$\text{MSE} = \frac{1}{NM} \sum_{i=1}^N \sum_{j=1}^M (I_{i,j} - \hat{I}_{i,j})^2.$$

PSNR is then computed from the MSE:

$$\text{PSNR} = 10 \cdot \log_{10} \left(\frac{\text{MAX}_I^2}{\text{MSE}} \right),$$

where MAX_I is the maximum possible pixel value of the image (e.g., 255 for 8-bit images).

To provide a perceptually aligned assessment, the SSIM is employed. SSIM measures luminance, contrast, and structure similarity between images and is defined as:

$$\text{SSIM}(I, \hat{I}) = \frac{(2\mu_I\mu_{\hat{I}} + C_1)(2\sigma_{I\hat{I}} + C_2)}{(\mu_I^2 + \mu_{\hat{I}}^2 + C_1)(\sigma_I^2 + \sigma_{\hat{I}}^2 + C_2)},$$

where μ_I and $\mu_{\hat{I}}$ are the means, σ_I^2 and $\sigma_{\hat{I}}^2$ are the variances, $\sigma_{I\hat{I}}$ is the covariance between I and \hat{I} , and C_1, C_2 are small constants to stabilize the division.

Recognizing the limitations of traditional metrics in capturing human-perceived quality, LPIPS metric is also employed. LPIPS compares deep feature activations from pre-trained neural networks, providing a score that correlates more strongly with subjective visual judgments. Given feature maps F_l from layer l of a neural network, LPIPS is computed as:

$$\text{LPIPS}(I, \hat{I}) = \sum_l w_l \left\| F_l(I) - F_l(\hat{I}) \right\|_2^2,$$

where w_l are learned weights and l indexes selected layers.

In addition to image quality, **inference time per batch** is recorded for all models. This enables a critical assessment of computational efficiency, which is an essential factor for practical deployment in real-world applications.

Results

Comparative results on CelebA-HQ (Karras et al. 2018) are presented in Table 1. CATformer achieves a performance competitive with, or outperformed, recent state-of-the-art SR approaches across most evaluation metrics. Notably, improvements in perceptual quality are reflected by lower LPIPS and higher SSIM scores, highlighting the effectiveness of the model in reconstructing both visual detail and structural similarity. In terms of computational efficiency, the proposed architecture exhibits inference speed and resource usage comparable to strong baseline methods, demonstrating that enhanced modeling capacity does not result in a significant increase in computational overhead.

Model	PSNR↑	SSIM↑	LPIPS↓	Time (s)
ESRGAN	29.33	0.7962	0.3133	<u>0.1415</u>
Real-ESRGAN	29.94	0.8221	0.2264	0.0788
SwinIR	29.82	0.8172	0.2323	0.4195
DiffBIR	26.94	0.7125	<u>0.2229</u>	2.3883
HAT	<u>31.83</u>	0.8424	0.3257	0.7554
CATformer	32.29	0.8921	0.1064	0.3379

Table 1: Comparison between the CATformer and state-of-the-art approaches on CelebA-HQ. The best metric result is highlighted in bold, and the second-best is underlined.

Across all evaluated datasets, the proposed method achieves consistently strong performance in both perceptual and structural quality metrics, often outperforming or

matching recent state-of-the-art approaches (an example output is shown in Figure 2). However, a moderate reduction in PSNR is observed on the DIV2K (Agustsson and Timofte 2017) and Urban100 (Huang, Singh, and Ahuja 2015) benchmarks. This reduction is consistent with the frequently reported trade-off between perceptual similarity and pixel-wise fidelity, as higher perceptual quality (reflected in LPIPS and SSIM) may sometimes come at the expense of lower PSNR values. Additionally, the results suggest that transformer- and GAN-based architectures may exhibit increased sensitivity to the size and diversity of the training dataset, potentially impacting generalization on certain domains. These observations highlight the need for further analysis and may motivate future refinement of architectural or training strategies to better balance perceptual and quantitative performance across a wider range of datasets.

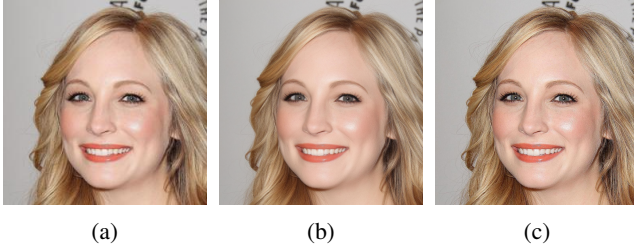


Figure 2: Visual comparison of results using CelebA-HQ dataset: (a) LR input, (b) CATformer result, and (c) HR Ground Truth (GT).

To provide a broader perspective on generalization and computational performance, Table 2 presents results on DIV2K and Urban100 datasets, reporting PSNR, SSIM, LPIPS, and run time per batch for the proposed approach and selected state-of-the-art baselines. Although CATformer maintains strong perceptual scores and efficient inference on most datasets, the margins of improvement vary and are not consistently substantial across all scenarios. These results reinforce the need for comprehensive evaluation and careful interpretation of cross-dataset generalizability.

Dataset	Method	PSNR \uparrow	SSIM \uparrow	LPIPS \downarrow	Time (s)
Div2k	ESRGAN	26.44	0.7703	<u>0.1151</u>	<u>0.4794</u>
	Real-ESRGAN	24.84	0.7307	0.2195	0.2909
	SwinIR	24.73	0.7314	0.2150	1.0518
	DiffBIR	22.95	0.6316	0.2464	8.5027
	HAT	29.61	<u>0.8553</u>	0.2331	2.1758
	CATformer	<u>27.39</u>	0.8632	0.0835	0.5490
	ESRGAN	<u>22.79</u>	0.7216	<u>0.1230</u>	<u>0.0968</u>
Urban100	Real-ESRGAN	21.06	0.6574	0.2139	0.0579
	SwinIR	21.02	0.6673	0.2014	0.4050
	DiffBIR	20.08	0.6060	0.2035	1.9867
	HAT	26.33	0.8304	0.1736	0.5975
	CATformer	20.93	<u>0.7407</u>	0.0772	0.2438

Table 2: Comparison of SSIM, LPIPS, and time per batch (s) between the CATformer and state-of-the-art approaches across five additional datasets. The best result for each metric is highlighted in bold, and the second-best is underlined.

A qualitative comparison of visual performance is presented in Figure 3, where the performance of CATformer is evaluated against ESRGAN, Real-ESRGAN, SwinIR, DiffBIR, and HAT. Taken together, the results highlight both the strengths and limitations of the CATformer approach. While notable improvements are achieved in perceptual quality and computational efficiency on these benchmarks, the less pronounced performance gains, particularly the observed reduction in PSNR on datasets such as Div2k, may be attributed to the model prioritizing perceptual realism at the expense of fidelity metrics. These observations underscore the importance of comprehensive evaluation across diverse conditions and point to the potential for further optimization. More research is needed, especially on how the scale and diversity of the data set influence the generalizability and robustness of the CATformer model.

Ablation Study

To assess the contribution of key architectural and optimization components, two ablation experiments were performed on the CelebA-HQ dataset. First, the learning rate was set to 1×10^{-5} instead of 1×10^{-4} to evaluate the sensitivity of the model to training dynamics. Results indicate that reducing the learning rate leads to slower convergence and a decrease in both perceptual and quantitative metrics, underscoring the importance of careful learning rate selection for stable and effective training. Second, the decoder was modified by removing not only the residual blocks but also all RRDB blocks, resulting in a purely convolutional upsampling pathway. This modification led to a noticeable decline in image quality, visually characterized by increased artifacts, blurriness, and noise. Quantitatively, this was reflected in a decrease in PSNR, despite an increase in SSIM and a lower LPIPS score (as shown in Table 3). These observations highlight the critical role of both residual and RRDB blocks play in reducing visual artifacts and preserving high-fidelity image reconstruction. Together, these findings demonstrate the significance of both appropriate optimization settings and architectural choices in achieving optimal SR performance.

Model Variant	PSNR \uparrow	SSIM \uparrow	LPIPS \downarrow	Time (s)
Different learning rate	30.19	0.7893	0.1382	0.34
Decoder w/o Res & RRDB	26.96	0.9343	0.0161	0.18
CATformer	32.29	0.8921	0.1064	0.34

Table 3: Ablation study on CelebA-HQ: evaluating the effect of latent noise injection (noise branch) and residual blocks in the decoder.

Discussion and Conclusion

This work presents CATformer, a model that unifies diffusion-inspired transformer modules, adversarial (GAN) learning, and contrastive learning for image super-resolution. Experimental results indicate that CATformer achieves better performance in perceptual metrics, structural similarity, and inference efficiency compared to leading

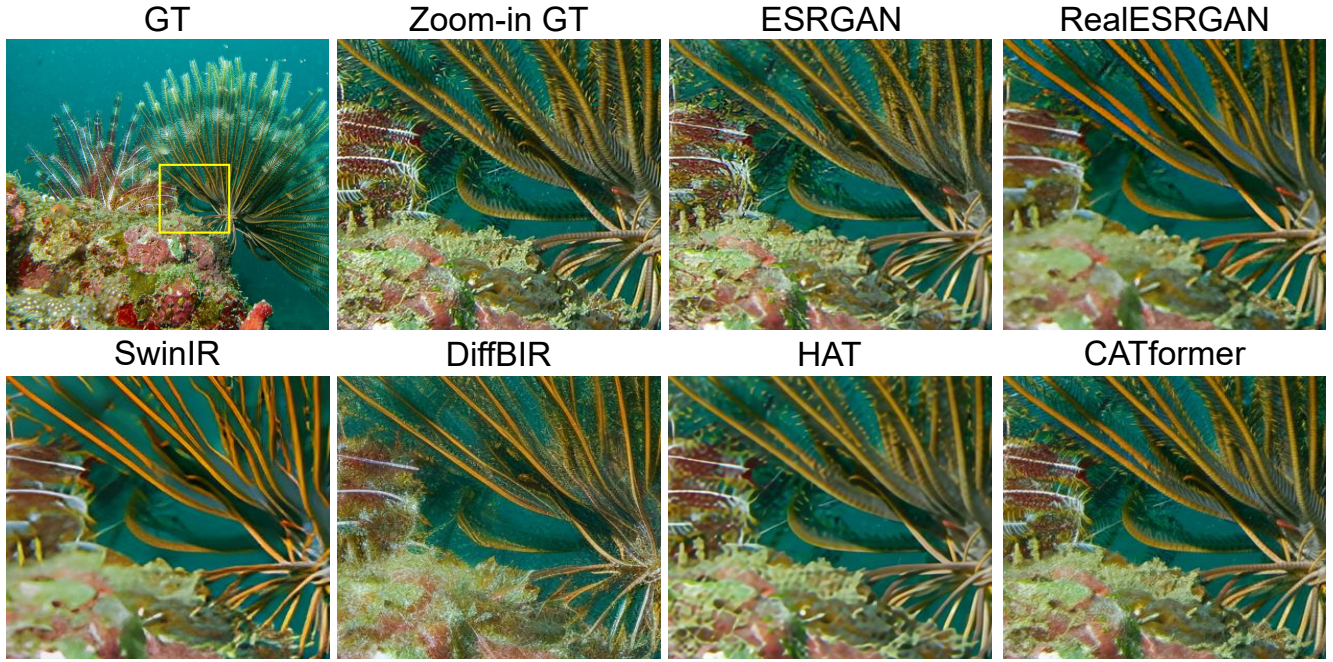


Figure 3: Qualitative comparison of visual performance.

diffusion- and transformer-based models. The findings from this study show that the dual-branch architecture enables robust feature extraction and the generation of visually realistic, high-quality images. Despite strong results in metrics such as Structural Similarity Index (SSIM), Learned Perceptual Image Patch Similarity (LPIPS), CATformer produces slightly lower Peak Signal-to-Noise Ratio (PSNR) scores than recent baselines, particularly on smaller datasets such as Urban100 and DIV2K. This outcome can be attributed both to the reliance of the architecture on large and diverse training data and to the inherent limitations of PSNR as an evaluation metric. PSNR quantifies the pixel-level difference between reconstructed and reference images, favoring outputs that minimize these differences. As a result, PSNR often rewards solutions that appear overly smooth and may not reflect improvements in perceptual sharpness, texture, or realism. Methods that incorporate adversarial and perceptual losses frequently generate images with higher visual fidelity according to human observers, even if PSNR scores are lower. Perceptual metrics such as SSIM and LPIPS provide a more reliable assessment of visual quality in these cases.

The findings from this study highlight both the strengths and current limitations of combining diffusion, transformer, GAN, and contrastive learning within a single super-resolution framework. CATformer demonstrates high effectiveness in scenarios where perceptual quality and structural integrity are critical. However, generalization to smaller or less diverse datasets remains a challenge due to the high capacity and data requirements of the architecture. Enhancement through data augmentation, semi-supervised learning, or regularization is recommended for future research. Plans

for code and model release will support reproducibility and further investigation by the research community. Overall, this study demonstrates that the integration of multiple generative and representation learning paradigms can advance the state of the art in image super-resolution, offering a robust foundation for future developments.

References

- Agustsson, E.; and Timofte, R. 2017. NTIRE 2017 Challenge on Single Image Super-Resolution: Dataset and Study. In *2017 IEEE Conference on Computer Vision and Pattern Recognition Workshops (CVPRW)*, 1122–1131.
- Blau, Y.; and Michaeli, T. 2018. The Perception-Distortion Tradeoff. In *2018 IEEE/CVF Conference on Computer Vision and Pattern Recognition*, 6228–6237. IEEE.
- Chen, X.; Wang, X.; Zhou, J.; Qiao, Y.; and Dong, C. 2023. Activating More Pixels in Image Super-Resolution Transformer. In *Proceedings of the IEEE/CVF Conference on Computer Vision and Pattern Recognition (CVPR)*, 22367–22377.
- Dosovitskiy, A.; Beyer, L.; Kolesnikov, A.; Weissenborn, D.; Zhai, X.; Unterthiner, T.; Dehghani, M.; Minderer, M.; Heigold, G.; Gelly, S.; Uszkoreit, J.; and Houlsby, N. 2021. An Image is Worth 16x16 Words: Transformers for Image Recognition at Scale. In *International Conference on Learning Representations*.
- He, Z.; Zhang, S.; Hu, R.; Shen, Y.; and Zhang, Y. 2025. BUFF: Bayesian Uncertainty Guided Diffusion Probabilistic Model for Single Image Super-Resolution. *Proceedings of the AAAI Conference on Artificial Intelligence*, 39(4): 3474–3482.

- Ho, J.; Saharia, C.; Chan, W.; Fleet, D. J.; Norouzi, M.; and Salimans, T. 2022. Cascaded Diffusion Models for High Fidelity Image Generation. *Journal of Machine Learning Research*, 23(47): 1–33.
- Huang, J.-B.; Singh, A.; and Ahuja, N. 2015. Single image super-resolution from transformed self-exemplars. In *2015 IEEE Conference on Computer Vision and Pattern Recognition (CVPR)*, 5197–5206.
- Karras, T.; Aila, T.; Laine, S.; and Lehtinen, J. 2018. Progressive Growing of GANs for Improved Quality, Stability, and Variation. In *International Conference on Learning Representations (ICLR)*.
- Kingma, D. P.; and Ba, J. 2015. Adam: A Method for Stochastic Optimization. In Bengio, Y.; and LeCun, Y., eds., *3rd International Conference on Learning Representations, ICLR 2015, San Diego, CA, USA, May 7-9, 2015, Conference Track Proceedings*.
- Kopeć, D.; Kozłowski, W.; Wizerkaniuk, M.; Krutul, D.; Kocoń, J.; and Zięba, M. 2025. SupResDiffGAN a new approach for the Super-Resolution task. arXiv:2504.13622.
- Ledig, C.; Theis, L.; Huszár, F.; Caballero, J.; Cunningham, A.; Acosta, A.; Aitken, A.; Tejani, A.; Totz, J.; Wang, Z.; and Shi, W. 2017. Photo-Realistic Single Image Super-Resolution Using a Generative Adversarial Network. In *2017 IEEE Conference on Computer Vision and Pattern Recognition (CVPR)*, 105–114.
- Li, J.; Wang, H.; Li, Y.; and Zhang, H. 2025. A Comprehensive Review of Image Restoration Research Based on Diffusion Models. *Mathematics*, 13(13).
- Liang, J.; Cao, J.; Sun, G.; Zhang, K.; Van Gool, L.; and Timofte, R. 2021. SwinIR: Image Restoration Using Swin Transformer. In *2021 IEEE/CVF International Conference on Computer Vision Workshops (ICCVW)*, 1833–1844.
- Lim, B.; Son, S.; Kim, H.; Nah, S.; and Lee, K. M. 2017. Enhanced Deep Residual Networks for Single Image Super-Resolution. In *2017 IEEE Conference on Computer Vision and Pattern Recognition Workshops (CVPRW)*, 1132–1140.
- Liu, Z.; Luo, P.; Wang, X.; and Tang, X. 2015. Deep Learning Face Attributes in the Wild. In *2015 IEEE International Conference on Computer Vision (ICCV)*, 3730–3738.
- Lu, Z.; Li, J.; Liu, H.; Huang, C.; Zhang, L.; and Zeng, T. 2022. Transformer for Single Image Super-Resolution. In *Proceedings of the IEEE/CVF Conference on Computer Vision and Pattern Recognition (CVPR) Workshops*, 457–466.
- Micikevicius, P.; Narang, S.; Alben, J.; Diamos, G.; Elsen, E.; Garcia, D.; Ginsburg, B.; Houston, M.; Kuchaiev, O.; Venkatesh, G.; and Wu, H. 2018. Mixed Precision Training. In *International Conference on Learning Representations*.
- Paszke, A.; Gross, S.; Massa, F.; Lerer, A.; Bradbury, J.; Chanan, G.; Killeen, T.; Lin, Z.; Gimelshein, N.; Antiga, L.; Desmaison, A.; Kopf, A.; Yang, E.; DeVito, Z.; Raison, M.; Tejani, A.; Chilamkurthy, S.; Steiner, B.; Fang, L.; Bai, J.; and Chintala, S. 2019. PyTorch: An Imperative Style, High-Performance Deep Learning Library. In Wallach, H.; Larochelle, H.; Beygelzimer, A.; d'Alché-Buc, F.; Fox, E.; and Garnett, R., eds., *Advances in Neural Information Processing Systems*, volume 32. Curran Associates, Inc.
- Peebles, W.; and Xie, S. 2023. Scalable Diffusion Models with Transformers. In *Proceedings of the IEEE/CVF International Conference on Computer Vision (ICCV)*, 4195–4205.
- Rombach, R.; Blattmann, A.; Lorenz, D.; Esser, P.; and Ommer, B. 2022. High-Resolution Image Synthesis With Latent Diffusion Models. In *Proceedings of the IEEE/CVF Conference on Computer Vision and Pattern Recognition (CVPR)*, 10684–10695.
- Ronneberger, O.; Fischer, P.; and Brox, T. 2015. U-Net: Convolutional Networks for Biomedical Image Segmentation. In Navab, N.; Hornegger, J.; Wells, W. M.; and Frangi, A. F., eds., *Medical Image Computing and Computer-Assisted Intervention – MICCAI 2015*, 234–241. Cham: Springer International Publishing. ISBN 978-3-319-24574-4.
- Saharia, C.; Ho, J.; Chan, W.; Salimans, T.; Fleet, D. J.; and Norouzi, M. 2023. Image Super-Resolution via Iterative Refinement. *IEEE Transactions on Pattern Analysis and Machine Intelligence*, 45(4): 4713–4726.
- Vaswani, A.; Shazeer, N.; Parmar, N.; Uszkoreit, J.; Jones, L.; Gomez, A. N.; Kaiser, L. u.; and Polosukhin, I. 2017. Attention is All you Need. In Guyon, I.; Luxburg, U. V.; Bengio, S.; Wallach, H.; Fergus, R.; Vishwanathan, S.; and Garnett, R., eds., *Advances in Neural Information Processing Systems*, volume 30. Curran Associates, Inc.
- Wang, L.; Wang, Y.; Dong, X.; Xu, Q.; Yang, J.; An, W.; and Guo, Y. 2021a. Unsupervised Degradation Representation Learning for Blind Super-Resolution. In *Proceedings of the IEEE/CVF Conference on Computer Vision and Pattern Recognition (CVPR)*, 10581–10590.
- Wang, X.; Xie, L.; Dong, C.; and Shan, Y. 2021b. Real-ESRGAN: Training Real-World Blind Super-Resolution with Pure Synthetic Data. In *2021 IEEE/CVF International Conference on Computer Vision Workshops (ICCVW)*, 1905–1914.
- Wang, X.; Yu, K.; Wu, S.; Gu, J.; Liu, Y.; Dong, C.; Qiao, Y.; and Loy, C. C. 2018. ESRGAN: Enhanced Super-Resolution Generative Adversarial Networks. In *Computer Vision – ECCV 2018 Workshops: Munich, Germany, September 8-14, 2018, Proceedings, Part V*, 63–79. Berlin, Heidelberg: Springer-Verlag. ISBN 978-3-030-11020-8.
- Wang, Y.; Jin, S.; Yang, Z.; Guan, H.; Ren, Y.; Cheng, K.; Zhao, X.; Liu, X.; Chen, M.; Liu, Y.; and Guo, Q. 2024. TTSR: A Transformer-Based Topography Neural Network for Digital Elevation Model Super-Resolution. *IEEE Transactions on Geoscience and Remote Sensing*, 62: 1–19.
- Wang, Z.; Bovik, A.; Sheikh, H.; and Simoncelli, E. 2004. Image quality assessment: from error visibility to structural similarity. *IEEE Transactions on Image Processing*, 13(4): 600–612.
- Wang, Z.; Chen, J.; and Hoi, S. C. H. 2021. Deep Learning for Image Super-Resolution: A Survey. *IEEE Transactions on Pattern Analysis and Machine Intelligence*, 43(10): 3365–3387.
- Wu, G.; Jiang, J.; and Liu, X. 2024. A Practical Contrastive Learning Framework for Single-Image Super-Resolution.

IEEE Transactions on Neural Networks and Learning Systems, 35(11): 15834–15845.

Yang, F.; Yang, H.; Fu, J.; Lu, H.; and Guo, B. 2020. Learning Texture Transformer Network for Image Super-Resolution. In *Proceedings of the IEEE/CVF Conference on Computer Vision and Pattern Recognition (CVPR)*.

Yue, L.; Shen, H.; Li, J.; Yuan, Q.; Zhang, H.; and Zhang, L. 2016. Image super-resolution: The techniques, applications, and future. *Signal Processing*, 128: 389–408.

Zamir, S. W.; Arora, A.; Khan, S.; Hayat, M.; Khan, F. S.; and Yang, M. 2022. Restormer: Efficient Transformer for High-Resolution Image Restoration. In *2022 IEEE/CVF Conference on Computer Vision and Pattern Recognition (CVPR)*, 5718–5729.

Zhang, R.; Isola, P.; Efros, A. A.; Shechtman, E.; and Wang, O. 2018. The Unreasonable Effectiveness of Deep Features as a Perceptual Metric. In *Proceedings of the IEEE Conference on Computer Vision and Pattern Recognition (CVPR)*.